

# An Efficient Method For Solving Highly Anisotropic Elliptic Equations

Edward Santilli<sup>a,\*</sup>, Alberto Scotti<sup>b</sup>

<sup>a</sup>*Dept. of Physics, 214 Phillips Hall, UNC, Chapel Hill, NC 27599*

<sup>b</sup>*Dept. of Marine Sciences, 3117H Venable Hall, UNC, Chapel Hill, NC 27599*

---

## Abstract

Solving elliptic PDEs in more than one dimension can be a computationally expensive task. For some applications characterised by a high degree of anisotropy in the coefficients of the elliptic operator, such that the term with the highest derivative in one direction is much larger than the terms in the remaining directions, the discretized elliptic operator often has a very large condition number – taking the solution even further out of reach using traditional methods. This paper will demonstrate a solution method for such ill-behaved problems. The high condition number of the  $D$ -dimensional discretized elliptic operator will be exploited to split the problem into a series of well-behaved one and  $(D - 1)$ -dimensional elliptic problems. This solution technique can be used alone on sufficiently coarse grids, or in conjunction with standard iterative methods, such as Conjugate Gradient, to substantially reduce the number of iterations needed to solve the problem to a specified accuracy. The solution is formulated analytically for a generic anisotropic problem using arbitrary coordinates, hopefully bringing this method into the scope of a wide variety of applications.

*Keywords:*

*PACS:* 02.60.Lj, 47.11.St

*2000 MSC:* 35J57, 65F10, 65F08, 65N22

---



---

\*Corresponding author

*Email addresses:* [santilli@physics.unc.edu](mailto:santilli@physics.unc.edu) (Edward Santilli), [ascotti@unc.edu](mailto:ascotti@unc.edu) (Alberto Scotti)

## Contents

<b>1</b>	<b>Introduction</b>	<b>3</b>
1.1	Notation . . . . .	6
<b>2</b>	<b>Derivation</b>	<b>7</b>
2.1	The desired form of the expansion . . . . .	8
2.2	Summary of the expansion . . . . .	13
2.3	Eliminating horizontal stages . . . . .	15
2.4	An interpretation of $\varepsilon$ . . . . .	17
<b>3</b>	<b>Convergence estimates</b>	<b>19</b>
3.1	Restricted case . . . . .	19
3.2	General case . . . . .	21
3.3	The leptic solver as a preconditioner . . . . .	22
<b>4</b>	<b>Demonstrations</b>	<b>25</b>
4.1	High leptic ratio - Cartesian coordinates . . . . .	27
4.2	Borderline cases - Cartesian coordinates . . . . .	27
4.3	High leptic ratio - Mapped coordinates . . . . .	30
4.4	Borderline case - Mapped coordinates . . . . .	32
<b>5</b>	<b>Discussion</b>	<b>33</b>

## 1. Introduction

The solution of Poisson problems is often the single most expensive step in the numerical solution of partial differential equations (PDEs). For example, when solving the Navier-Stokes or Euler equations, the Poisson problem arises from the incompressibility condition [1, 2]. The particular solution strategy depends of course on a combination of factors, including the specific choice of the discretization and the type of boundary conditions. In simple geometries, very efficient schemes can be devised to reduce the effective dimensionality of the problem, such as using FFTs or cyclic reduction to partially or completely diagonalize the operator [2]. For more complex geometries or boundary conditions, the available choices to solve the discretized problem usually involves direct inversion for small size problems, while Krylov based iterative methods such as Conjugate Gradient or multigrid methods are used when the matrix problem is too large to be inverted exactly [2, 3, 4].

In this paper, we are interested in Poisson problems characterized by a high level of anisotropy (to be precisely defined later). The source of anisotropy can be due to the highly flattened domains over which the solution is sought, as is the case for atmospheric, oceanic [2] and some astrophysical problems [5, p. 77]. However, the source of anisotropy could have a physical base, e.g. Non-Fickian diffusion problems where the flux is related to the gradient by an anisotropic tensor [6]. Recently, research has been conducted to develop compound materials that could serve as a cloaking device. [7, 8] These *metamaterials* are designed to have specific anisotropic acoustic and electromagnetic properties that divert pressure and light waves around a region of space unscathed.

Anisotropy results in a spreading of the spectrum of the discretized operator, with severe consequences on the convergence rate. We illustrate this point with a simple Poisson problem

$$\nabla^2 \phi = \rho.$$

The r.h.s. and boundary conditions are chosen randomly (but compatible, see below). The Laplacian operator is discretized with a standard 7-point, second-

order stencil, the domain is rectangular with dimensions  $L \times L \times H$ , the domain's aspect ratio is measured by  $R = L/H$ , and the discretization is chosen as  $(\Delta x, \Delta y, \Delta z) = (H/2, H/2, H/16)$ . For illustration purposes, the problem is solved using a 4-level multigrid scheme which employs line relaxation in the vertical (stiff) direction, as used by Armenio and Roman [9] to do a LES of a shallow coastal area. Figure 1 shows the attenuation factor  $A = \|E_{n+1}\|/\|E_n\|$  as a function of the aspect ratio, where  $E_n$  is the residual error after  $n$  iterations. For moderate aspect-ratio domains, the convergence is satisfactory, but as  $R$  increases, we rapidly approach a point where the method becomes, for practical purposes, useless. Similar results (see below) hold for Krylov based methods.

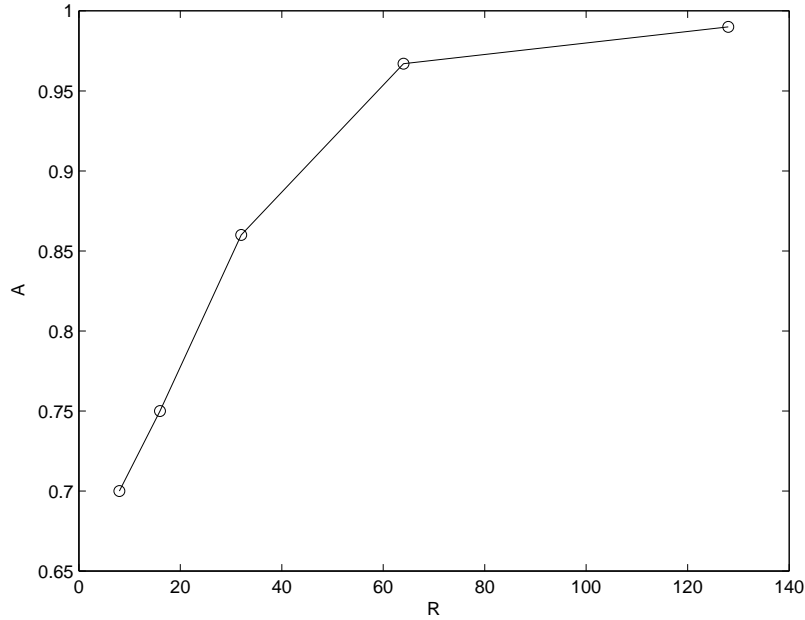


Figure 1: Attenuation factor as a function of domain aspect ratio for a Poisson problem solved using a standard multigrid scheme.

In this paper, we describe how a formal series solution of a Poisson problem derived by Scotti and Mitran [10], herein referred to as SM, can be used to significantly speed up the convergence of traditional iterative schemes. SM in-

roduced the concept of grid lepticity,  $\lambda$ , to describe the degree of anisotropy of a discretized domain and then sought a solution to the Poisson problem written as a power series in  $\lambda^{-1}$  – the leptic expansion. An apparent limitation of the leptic expansion is that it is very efficient only for lepticity larger than a critical value of order 1. SM were led to introduce the leptic expansion in order to provide the right amount of dispersion needed to balance nonlinear steepening of internal waves propagating in a shallow stratified ocean. For this limited purpose, SM showed that at most only three terms in the expansion are needed, and thus the lack of overall convergence was not a serious limitation. Here, we develop the method for the purpose of efficiently calculating solutions of a discretized Poisson problem. In our approach, the lepticity, which in SM’s original formulation was related to the aspect ratio of the domain, becomes now a generic measure of anisotropy. The main result of this paper is that for subcritical values of the lepticity, the leptic expansion can still be extremely valuable to dramatically increase the convergence rate of standard iterative schemes, as the numerical demonstrations of the method will show. The examples are coded using Matlab and Chombo’s BoxTools<sup>1</sup> library with standard second order discretization techniques.

What makes the leptic expansion particularly attractive is that it can be parallelized in a very straightforward way, as long as the decomposition of the domain does not split along the stiff (vertical, in our examples) direction. For comparison, the parallel implementation of the Incomplete Cholesky Decomposition of a sparse matrix, which is used as a preconditioner for Conjugate Gradient schemes and yields very good convergence rates even at high levels of anisotropy [11], is a highly non-trivial task [12].

Finally, it must be noted that the idea behind the leptic expansion can be traced as far back as the work of Bousinnesq on waves [13]. What we have done here is to formulate it in a way suitable for numerical calculations.

---

<sup>1</sup>Chombo has been developed and is being distributed by the Applied Numerical Algorithms Group of Lawrence Berkeley National Lab. Website: <https://seesar.lbl.gov/ANAG/chombo/>

The rest of the paper is organized as follows: a discretization- and coordinate-independent version of the leptic expansion is introduced in Section 2. The reader who is not interested in the details may skip directly to Section 2.2, where a summary of the scheme is provided. Section 3 presents convergence estimates of the leptic expansion using Fourier analysis techniques [14]. This is where the leptic method's potential to generate initial guesses for conventional iterative schemes emerges. In Section 4, we consider some examples to illustrate how the leptic expansion can be used with conventional iterative schemes to create very efficient solvers. A final section summarizes the main results.

### 1.1. Notation

As an aid to the following discussion, we define the relevant notation here.

- Horizontal coordinate directions:  $x^1 = x, x^2 = y$ . Vertical (stiff) coordinate direction:  $x^3 = z$ .
- $H$  = vertical domain extent.  $L$  = horizontal domain extent.
- $\phi$  = full solution.  $\phi_p$  = solution of  $p^{\text{th}}$ -order equation.
- $\phi^v$  and  $\phi^h$  = solution of vertical and horizontal equations (explained in section 2).
- Summation indices<sup>2</sup> (summed from 1 to 3):  $i, j$ .
- Horizontal summation indices (summed from 1 to 2):  $m, n$ .
- $u^{\star i} = (u^{\star}, v^{\star}, w^{\star})^i$ , the flux field that will be used as Neumann boundary conditions.
- $\rho$  = the source term of the elliptic PDE.
- $\sigma^{ij}$  = a symmetric, contravariant tensor field.

---

<sup>2</sup>I will use summation notation. Repeated indices imply a sum unless explicitly stated otherwise.

- $\mathcal{V}$  is the 3-dimensional domain and  $d\mathcal{V} = dx^1 dx^2 dx^3$ .
- $\mathcal{A}_i$  is the boundary of  $\mathcal{V}$  in the  $i^{\text{th}}$ -direction.
- $d\mathcal{A}_i = (dx^2 dx^3, dx^3 dx^1, dx^1 dx^2)_i^T$ , the area element at the boundary of  $\mathcal{V}$ .
- $\mathcal{S}$  is the 2-dimensional horizontal domain with local coordinates  $(x^1, x^2)$  and  $d\mathcal{S} = dx^1 dx^2$ .
- $dl_m = (dx^1, dx^2)_m^T$ , the line element around the boundary of  $\mathcal{S}$ .
- $\bar{A}(x, y) = \frac{1}{H} \int_{z_-}^{z_+} A(x, y, z) dz$ , the vertical average of  $A$ .
- The leptic ratio is defined as  $\lambda = \Delta x / H$ , where  $\Delta x$  is the horizontal mesh spacing.

## 2. Derivation

The problem we wish to solve is an anisotropic elliptic PDE with Neumann boundary conditions of the type that often arises when solving the incompressible Navier-Stokes equations [1, 2]. More precisely, we wish to solve the following equation

$$\begin{aligned} \partial_i \sigma^{ij} \partial_j \phi &= \rho \text{ in } \mathcal{V} \\ \sigma^{ij} \partial_j \phi &= u^{*i} \text{ on } \partial\mathcal{V}, \end{aligned} \tag{1}$$

where  $\sigma^{ij}$  is a positive-definite, symmetric tensor field. The only restriction on  $\rho$  and  $u^{*i}$  is that they must be compatible with one another. That is, if we integrate eq. (1) over  $\mathcal{V}$  and apply Stokes' theorem, we obtain an identity that must be obeyed by the sources,

$$\int_{\mathcal{V}} \rho d\mathcal{V} = \oint_{\partial\mathcal{V}} u^{*i} d\mathcal{A}_i. \tag{2}$$

In general, the domain can have any number of dimensions higher than 1, but without loss of generality we will restrict ourselves to the 3-dimensional case. We will also assume there is a small parameter,  $\varepsilon$ , that we can use to

identify terms of the field and operator in a formal perturbation expansion of the form

$$\begin{aligned}\phi &= \phi_0 + \varepsilon \phi_1 + \varepsilon^2 \phi_2 + \varepsilon^3 \phi_3 + \dots \\ \partial_i \sigma^{ij} \partial_j &= \partial_3 \sigma^{33} \partial_3 + \varepsilon (\partial_m \sigma^{mn} \partial_n + \partial_m \sigma^{m3} \partial_3 + \partial_3 \sigma^{3n} \partial_n) .\end{aligned}\tag{3}$$

In this section, we will derive a method to solve eqs. (1) using the expansion (3).

### 2.1. The desired form of the expansion

We begin by plugging expansion (3) into the first of eqs. (1) and equating powers of  $\varepsilon$ .

$$\partial_3 \sigma^{33} \partial_3 \phi_0 = \rho \tag{4}$$

$$\partial_3 \sigma^{33} \partial_3 \phi_1 + (\partial_m \sigma^{m3} \partial_3 + \partial_3 \sigma^{3n} \partial_n + \partial_m \sigma^{mn} \partial_n) \phi_0 = 0 \tag{5}$$

$$\partial_3 \sigma^{33} \partial_3 \phi_2 + (\partial_m \sigma^{m3} \partial_3 + \partial_3 \sigma^{3n} \partial_n + \partial_m \sigma^{mn} \partial_n) \phi_1 = 0 \tag{6}$$

etc...

The first thing to notice is that eq. (4) with Neumann boundary conditions can only determine  $\phi_0$  up to an additive function of  $x$  and  $y$ . We will call the solution of eq. (4)  $\phi_0^v(x, y, z)$  and the still undetermined function  $\phi_0^h(x, y)$ . We might as well preemptively write the fields at every order as

$$\phi_n(x, y, z) = \phi_n^v(x, y, z) + \phi_n^h(x, y)$$

so that equations (4)-(6) read

$$\partial_3 \sigma^{33} \partial_3 \phi_0^v = \rho \tag{7}$$

$$\partial_3 \sigma^{33} \partial_3 \phi_1^v + \partial_m \sigma^{m3} \partial_3 \phi_0^v + (\partial_3 \sigma^{3n} \partial_n + \partial_m \sigma^{mn} \partial_n) \phi_0^v = 0 \tag{8}$$

$$\partial_3 \sigma^{33} \partial_3 \phi_2^v + \partial_m \sigma^{m3} \partial_3 \phi_1^v + (\partial_3 \sigma^{3n} \partial_n + \partial_m \sigma^{mn} \partial_n) \phi_1^v = 0 \tag{9}$$

etc...



In order to solve this set of equations, we must define our boundary conditions at each order. At  $\mathcal{O}(1)$ , we will set

$$\begin{aligned}\sigma^{33}\partial_3\phi_0^v|_{z_+} &= w^*|_{z_+} - \tilde{w}_0 \\ \sigma^{33}\partial_3\phi_0^v|_{z_-} &= w^*|_{z_-},\end{aligned}$$

where  $z_+$  and  $z_-$  denote the evaluation at the upper and lower boundaries, respectively. The excess function,  $\tilde{w}_0$ , is defined at each  $x$  and  $y$  to make eq. (7) consistent with its boundary conditions. By vertically integrating eq. (7), we see that

$$\begin{aligned}\int_{z_-}^{z_+} \rho dz &= \sigma^{33}\partial_3\phi_0^v|_{z_-}^{z_+} \\ &= w^*|_{z_-}^{z_+} - \tilde{w}_0,\end{aligned}$$

that is,

$$\tilde{w}_0 = w^*|_{z_-}^{z_+} - \int_{z_-}^{z_+} \rho dz.$$

This completely determines  $\phi_0^v$  along vertical lines at each  $x$  and  $y$ . Notice that we have not yet chosen the gradients of  $\phi_0^v$  normal to the horizontal boundaries. We will save this freedom for later. Right now, we need to look at the  $\mathcal{O}(\varepsilon)$  equations to get  $\phi_0^h$ .

For the moment, let us think of eq. (8) as an equation for  $\phi_1^v$ . We again need to specify vertical boundary conditions. We will define

$$\begin{aligned}\sigma^{33}\partial_3\phi_1^v|_{z_+} &= \tilde{w}_0 - \sigma^{3n}\partial_n\phi_0|_{z_+} \\ \sigma^{33}\partial_3\phi_1^v|_{z_-} &= -\sigma^{3n}\partial_n\phi_0|_{z_-}.\end{aligned}\tag{10}$$

Defining a new excess function is unnecessary because it can just be absorbed into the still undetermined function  $\phi_0^h$ . As before, we vertically integrate eq.

(8).

$$\begin{aligned}
0 &= [\sigma^{33}\partial_3\phi_1^v + \sigma^{3n}\partial_n\phi_0]_{z_-}^{z_+} + \int_{z_-}^{z_+} (\partial_m\sigma^{m3}\partial_3\phi_0^v + \partial_m\sigma^{mn}\partial_n\phi_0) dz \\
&= \tilde{w}_0 + \int_{z_-}^{z_+} (\partial_m\sigma^{m3}\partial_3\phi_0^v + \partial_m\sigma^{mn}\partial_n\phi_0) dz \\
&= \tilde{w}_0 + \int_{z_-}^{z_+} (\partial_m\sigma^{m3}\partial_3\phi_0^v + \partial_m\sigma^{mn}\partial_n\phi_0^v) dz + \int_{z_-}^{z_+} \partial_m\sigma^{mn}\partial_n\phi_0^h dz \\
&= \tilde{w}_0 + \int_{z_-}^{z_+} \partial_m\sigma^{mj}\partial_j\phi_0^v dz + \int_{z_-}^{z_+} \partial_m\sigma^{mn}\partial_n\phi_0^h dz
\end{aligned}$$

If we divide by  $H$ , the vertical integrals become vertical averages, which will be denoted with overbars. When taking these averages, remember that while  $\phi^h$  was defined to be independent of  $z$ , no such assumption was made for  $\sigma^{ij}$ . This leaves us with an equation for  $\phi_0^h$ ,

$$\partial_m\overline{\sigma^{mn}}\partial_n\phi_0^h = -\frac{\tilde{w}_0}{H} - \partial_m\overline{\sigma^{mj}}\partial_j\phi_0^v. \quad (11)$$

If  $\phi_0^h$  is chosen to be any solution to this equation, then eq. (8) for  $\phi_1^v$  together with the boundary conditions (10) will be consistent. Now, we define boundary conditions for eq. (11) to be

$$\overline{\sigma^{mn}}\partial_n\phi_0^h|_{\vec{x}\in\partial\mathcal{S}} = \overline{u^{*m}}|_{\vec{x}\in\partial\mathcal{S}}. \quad (12)$$

This choice of boundary condition will be made consistent with equation (11) in the following steps. First, we integrate eq. (11) over  $\mathcal{S}$  and reorganize the result.

$$\begin{aligned}
-\frac{1}{H}\int_{\mathcal{S}}\tilde{w}_0 d\mathcal{S} - \oint_{\partial\mathcal{S}}\overline{\sigma^{mj}}\partial_j\phi_0^v dl_m &= -\int_{\mathcal{S}}\frac{\tilde{w}_0}{H} d\mathcal{S} - \int_{\mathcal{S}}\partial_m\overline{\sigma^{mj}}\partial_j\phi_0^v d\mathcal{S} \\
&= \int_{\mathcal{S}}\partial_m\overline{\sigma^{mn}}\partial_n\phi_0^h d\mathcal{S} \\
&= \oint_{\partial\mathcal{S}}\overline{\sigma^{mn}}\partial_n\phi_0^h dl_m \\
&= \oint_{\partial\mathcal{S}}\overline{u^{*m}} dl_m
\end{aligned}$$

Next, we exploit the remaining freedoms in the boundary conditions of  $\phi_0^v$  by choosing  $\sigma^{mj}\partial_j\phi_0^v = u^{*m} - \overline{u^{*m}}$  at the horizontal boundaries of  $\mathcal{V}$ . This, together

with the definition of  $\tilde{w}_0$ , gives us

$$-\frac{1}{H} \int_{\mathcal{S}} \left( w^*|_{z_-}^{z_+} - \int_{z_-}^{z_+} \rho dz \right) d\mathcal{S} - \oint_{\partial\mathcal{S}} \overline{(u^{*m} - \overline{u^{*m}})} dl_m = \oint_{\partial\mathcal{S}} \overline{u^{*m}} dl_m.$$

Noting that the third and fourth terms cancel, this simplifies to become

$$H \oint_{\partial\mathcal{S}} \overline{u^{*m}} dl_m + \int_{\mathcal{S}} w^*|_{z_-}^{z_+} d\mathcal{S} = \int_{\mathcal{V}} \rho d\mathcal{V}.$$

Now, if this equation holds, then the boundary conditions (12) will be consistent with the horizontal equation (11). From equation (2), we see that this is indeed the case. Therefore, equations (11) and (12) completely determine  $\phi_0^h$ , and in turn,  $\phi_0$ . Having  $\phi_0$  at our disposal, we can now tidy up eq. (8) a bit.

$$\begin{aligned} \partial_3 \sigma^{33} \partial_3 \phi_1^v &= -\partial_m \sigma^{m3} \partial_3 \phi_0^v - (\partial_m \sigma^{mn} \partial_n + \partial_3 \sigma^{3n} \partial_n) \phi_0 \\ &= (\rho - \partial_3 \sigma^{33} \partial_3 \phi_0) - \partial_m \sigma^{m3} \partial_3 \phi_0 - (\partial_m \sigma^{mn} \partial_n + \partial_3 \sigma^{3n} \partial_n) \phi_0 \\ &= \rho - \partial_i \sigma^{ij} \partial_j \phi_0 \end{aligned}$$

The first two terms in parentheses in the second line are zero via eq. (7). Since this equation along with boundary conditions (10) are consistent, this completely determines  $\phi_1^v$  at each  $x$  and  $y$ . There is, as before, another freedom yet to be chosen – the gradients of  $\phi_1^v$  normal to the horizontal boundaries. Again, we will choose them later.

We continue in the same manner, obtaining an equation for  $\phi_2^v$  whose Neumann compatibility condition is the equation for  $\phi_1^h$ . At this point, we might as well just derive the equations for the general order fields  $\phi_p^v$  and  $\phi_{p-1}^h$  where  $p \geq 2$ . We start with

$$\partial_3 \sigma^{33} \partial_3 \phi_p^v + \partial_m \sigma^{m3} \partial_3 \phi_{p-1}^v + (\partial_m \sigma^{mn} \partial_n + \partial_3 \sigma^{3n} \partial_n) \phi_{p-1} = 0 \quad (13)$$

and the vertical boundary conditions for  $\phi_p^v$

$$\sigma^{33} \partial_3 \phi_p^v|_{z_{\pm}} = -\sigma^{3n} \partial_n \phi_{p-1}|_{z_{\pm}}.$$

Vertically averaging eq. (13) and rearranging a bit gives us

$$\frac{1}{H} [\sigma^{33} \partial_3 \phi_p^v + \sigma^{3n} \partial_n \phi_{p-1}]_{z_-}^{z_+} + \overline{\partial_m \sigma^{mj} \partial_j \phi_{p-1}^v + \partial_m \sigma^{mn} \partial_n \phi_{p-1}^h} = 0,$$

which upon applying boundary conditions and rearranging some more gives us the horizontal equation

$$\partial_m \overline{\sigma^{mn}} \partial_n \phi_{p-1}^h = -\partial_m \overline{\sigma^{mj} \partial_j \phi_{p-1}^v}. \quad (14)$$

This equation will be compatible with homogeneous boundary conditions if we chose the gradients of  $\phi_p^v$  at the horizontal boundaries wisely. By integrating eq. (14) over  $\mathcal{S}$ , we find

$$\begin{aligned} 0 &= \oint_{\partial \mathcal{S}} \overline{\sigma^{mn}} \partial_n \phi_{p-1}^h dl_m \\ &= \int_{\mathcal{S}} \partial_m \overline{\sigma^{mn}} \partial_n \phi_{p-1}^h d\mathcal{S} \\ &= - \int_{\mathcal{S}} \partial_m \overline{\sigma^{mj} \partial_j \phi_{p-1}^v} d\mathcal{S} \\ &= - \oint_{\partial \mathcal{S}} \overline{\sigma^{mj} \partial_j \phi_{p-1}^v} dl_m. \end{aligned}$$

It is tempting now to let the gradients of  $\phi_{p-1}^v$  for  $p \geq 2$  be identically zero, but a more appropriate choice is

$$\sigma^{mj} \partial_j \phi_{p-1}^v = (\overline{\sigma^{mn}} - \sigma^{mn}) \partial_n \phi_{p-2}^h, \quad (15)$$

which is equivalent to

$$\sigma^{mj} \partial_j \phi_p^v = \begin{cases} \overline{u^{*m}} - \sigma^{mn} \partial_n \phi_0^h, & p = 1 \\ -\sigma^{mn} \partial_n \phi_{p-1}^h, & p \geq 2. \end{cases}$$

This choice will average to zero, satisfying the above integral, as well as prevent inconsistencies later.

Finally, we can clean up eq. (13) to get an equation for  $\phi_p^v$ .

$$\partial_3 \sigma^{33} \partial_3 \phi_p^v = \rho - \partial_i \sigma^{ij} \partial_j (\phi_0 + \phi_1 + \dots + \phi_{p-1})$$

This completes the derivation of the needed equations. It may seem like some of the boundary conditions were chosen only to be compatible with their corresponding differential equation, when in fact we chose them carefully so that the sum of their contributions is  $u^{*i}$  for each direction,  $i$ . At the horizontal

boundaries,

$$\begin{aligned}
\sigma^{mj}\partial_j\phi &= (\sigma^{mj}\partial_j\phi_0^v) + (\sigma^{mn}\partial_n\phi_0^h + \sigma^{mj}\partial_j\phi_1^v) + \dots + (\sigma^{mn}\partial_n\phi_{p-1}^h + \sigma^{mj}\partial_j\phi_p^v) + \dots \\
&= (u^{\star m} - \overline{u^{\star m}}) + (\overline{\sigma^{mn}}\partial_n\phi_0^h) + \dots + (\overline{\sigma^{mn}}\partial_n\phi_{p-1}^h) + \dots \\
&= (u^{\star m} - \overline{u^{\star m}}) + (\overline{u^{\star m}}) + \dots + (0) + \dots \\
&= u^{\star m},
\end{aligned}$$

at the upper vertical boundary,

$$\begin{aligned}
\sigma^{3j}\partial_j\phi|_{z_+} &= (\sigma^{33}\partial_3\phi_0^v) + (\sigma^{3n}\partial_n\phi_0 + \sigma^{33}\partial_3\phi_1^v) + \dots + (\sigma^{3n}\partial_n\phi_{p-1} + \sigma^{33}\partial_3\phi_p^v) + \dots \\
&= (w^\star - \tilde{w}_0) + (\tilde{w}_0) + \dots + (0) + \dots \\
&= w^\star,
\end{aligned}$$

and at the lower vertical boundary,

$$\begin{aligned}
\sigma^{3j}\partial_j\phi|_{z_-} &= (\sigma^{33}\partial_3\phi_0^v) + (\sigma^{3n}\partial_n\phi_0 + \sigma^{33}\partial_3\phi_1^v) + \dots + (\sigma^{3n}\partial_n\phi_{p-1} + \sigma^{33}\partial_3\phi_p^v) + \dots \\
&= (w^\star) + (0) + \dots + (0) + \dots \\
&= w^\star.
\end{aligned}$$

## 2.2. Summary of the expansion

Tables (1) and (2) provide a concise overview of the steps involved in generating the  $n^{th}$ -order of the expansion in generalized and Cartesian coordinates, respectively. The problem is formulated recursively. The left hand side is the same at each step. However, it must be noted that the solution of the  $(D-1)$ -dimensional Poisson problem can be postponed or in some cases eliminated depending on the magnitude of the correction required. This will be discussed in section 2.3. For a very simple example problem solved using this expansion, see section 3.

$\mathcal{O}(1)$	$\partial_3 \sigma^{33} \partial_3 \phi_0^v = \rho$	$\sigma^{33} \partial_3 \phi_0^v _{z_{\pm}} = \begin{cases} w^* _{z_+} - \tilde{w}_0, & z = z_+ \\ w^* _{z_-}, & z = z_- \end{cases}$ $\sigma^{mj} \partial_j \phi_0^v _{\vec{x} \in \mathcal{A}_m} = [u^{*m} - \overline{u^{*m}}]_{\vec{x} \in \mathcal{A}_m}$
	$\partial_m \overline{\sigma^{mn}} \partial_n \phi_0^h = -\frac{\tilde{w}_0}{H} - \partial_m \overline{\sigma^{mj} \partial_j \phi_0^v}$	$\overline{\sigma^{mn}} \partial_n \phi_0^h _{\vec{x} \in \partial \mathcal{S}} = \overline{u^{*m}} _{\vec{x} \in \partial \mathcal{S}}$
$\mathcal{O}(\varepsilon)$	$\partial_3 \sigma^{33} \partial_3 \phi_1^v = \rho - \partial_i \sigma^{ij} \partial_j \phi_0$	$\sigma^{33} \partial_3 \phi_1^v _{z_{\pm}} = \begin{cases} \tilde{w}_0 - \sigma^{3n} \partial_n \phi_0 _{z_+}, & z = z_+ \\ -\sigma^{3n} \partial_n \phi_0 _{z_-}, & z = z_- \end{cases}$ $\sigma^{mj} \partial_j \phi_1^v _{\vec{x} \in \mathcal{A}_m} = [\overline{u^{*m}} - \sigma^{mn} \partial_n \phi_0^h]_{\vec{x} \in \mathcal{A}_m}$
	$\partial_m \overline{\sigma^{mn}} \partial_n \phi_1^h = -\partial_m \overline{\sigma^{mj} \partial_j \phi_1^v}$	$\overline{\sigma^{mn}} \partial_n \phi_1^h _{\vec{x} \in \partial \mathcal{S}} = 0$
$\mathcal{O}(\varepsilon^p)$	$\partial_3 \sigma^{33} \partial_3 \phi_p^v = \rho - \partial_i \sigma^{ij} \partial_j \left( \sum_{r=0}^{p-1} \phi_r \right)$	$\sigma^{33} \partial_3 \phi_p^v _{z_{\pm}} = -\sigma^{3n} \partial_n \phi_{p-1} _{z_{\pm}}$ $\sigma^{mj} \partial_j \phi_p^v _{\vec{x} \in \mathcal{A}_m} = -\sigma^{mn} \partial_n \phi_{p-1}^h _{\vec{x} \in \mathcal{A}_m}$
	$\partial_m \overline{\sigma^{mn}} \partial_n \phi_p^h = -\partial_m \overline{\sigma^{mj} \partial_j \phi_p^v}$	$\overline{\sigma^{mn}} \partial_n \phi_p^h _{\vec{x} \in \partial \mathcal{S}} = 0$

Table 1: The general form of the expansion. The indices  $i, j$  extend over all directions and the indices  $m, n$  do not include the vertical (thin) direction. The excess function is defined as  $\tilde{w}_0 = w^*|_{z_-}^{z_+} - \int_{z_-}^{z_+} \rho dz$ .

$\mathcal{O}(1)$	$\partial_z^2 \phi_0^v = \rho$	$\partial_z \phi_0^v _{z_{\pm}} = \begin{cases} w^{\star} _{z_+} - \tilde{w}_0, & z = z_+ \\ w^{\star} _{z_-}, & z = z_- \end{cases}$ $\partial_m \phi_0^v _{\vec{x} \in \mathcal{A}_m} = [u^{\star m} - \overline{u^{\star m}}]_{\vec{x} \in \mathcal{A}_m}$
	$\nabla_h^2 \phi_0^h = -\frac{\tilde{w}_0}{H}$	$\partial_m \phi_0^h _{\vec{x} \in \partial S} = \overline{u^{\star m}} _{\vec{x} \in \partial S}$
$\mathcal{O}(\varepsilon)$	$\partial_z^2 \phi_1^v = \rho - \nabla^2 \phi_0$	$\partial_z \phi_1^v _{z_{\pm}} = \begin{cases} \tilde{w}_0, & z = z_+ \\ 0, & z = z_- \end{cases}$ $\partial_m \phi_1^v _{\vec{x} \in \mathcal{A}_m} = 0$
	No horizontal equation. $\phi_1^h = 0$	
$\mathcal{O}(\varepsilon^p)$	$\partial_z^2 \phi_p^v = \rho - \nabla^2 \left( \sum_{r=0}^{p-1} \phi_r \right)$	$\partial_z \phi_p^v _{z_{\pm}} = 0$ $\partial_m \phi_p^v _{\vec{x} \in \mathcal{A}_m} = 0$
	No horizontal equation. $\phi_p^h = 0$	

Table 2: The expansion in Cartesian coordinates. The indices  $i, j$  extend over all directions and the indices  $m, n$  do not include the vertical (thin) direction. The excess function is defined as  $\tilde{w}_0 = w^{\star}|_{z_-}^{z_+} - \int_{z_-}^{z_+} \rho dz$  and the horizontal Laplacian is  $\nabla_h^2 = \partial_x^2 + \partial_y^2$ .

### 2.3. Eliminating horizontal stages

Typically, solutions of the horizontal problems are more expensive than solutions of the vertical problems. Sometimes, we can skip the horizontal stages altogether if we know in advance that its solution will not contribute to the

overall convergence of the method. For example, suppose

$$\sigma^{ij} = \begin{pmatrix} A(x, y) & D(x, y) & 0 \\ D(x, y) & B(x, y) & 0 \\ 0 & 0 & C(x, y, z) \end{pmatrix}$$

where  $A, B, C$ , and  $D$  are arbitrary functions of the variables listed. We see that

$$\partial_m \overline{\sigma^{mj} \partial_j \phi^v} = \partial_m \sigma^{mn} \partial_n \overline{\phi^v} + \partial_m \sigma^{m3} \overline{\partial_3 \phi^v},$$

but since  $\sigma^{m3} = 0$  by assumption, the  $\partial_m \sigma^{m3} \overline{\partial_3 \phi^v}$  term is zero. Also, since each  $\phi_p^v$  is the solution of an ordinary differential equation with Neumann BCs, we can choose solutions whose vertical averages are zero – eliminating the  $\partial_m \sigma^{mn} \partial_n \overline{\phi^v}$  term as well. This means that the r.h.s. of the horizontal equations become zero for all but the  $\mathcal{O}(1)$  stages. Since the boundary conditions are also zero for these problems, the solutions,  $\phi_{p \geq 1}^h$ , must be identically zero. Whenever  $\sigma^{ij}$  has this form,  $\phi_0^h$  is the only horizontal function that needs to be found – eliminating most of the computation time.

In practice,  $\sigma^{ij}$  is often very close to the form shown above. In fact, many useful coordinate systems such as the Cartesian, cylindrical, and spherical systems are described by  $\sigma^{ij} = \sqrt{g} g^{ij}$  which are *exactly* of this form. It is helpful to consider this while iterating. If we can find a value of  $P$  such that all  $\phi_{p \geq P}^h$  will not significantly influence the overall convergence, or if we calculate that the norm of the horizontal equation's r.h.s. is below some threshold, then we can tell the leptic solver to stop performing horizontal solves in the interest of computation time. Alternatively, suppose we are about to find  $\phi_p^h$ . We could simply set  $\phi_p^h$  to zero everywhere and then set up the next vertical stage. If the vertical problem is consistent up to some prescribed tolerance, then we never needed the true solution of the horizontal equation to begin with! Otherwise, we can go back and solve the horizontal equation before moving on to the next vertical stage. This is a very economical way of deciding which horizontal solves are necessary.



#### 2.4. An interpretation of $\varepsilon$

So far, we have derived a set of equations that produce a formal solution to the original Poisson problem based on the assumption that the parameter  $\varepsilon$  in eqs. (3) properly identifies terms of fundamentally different sizes. The procedure does not refer to a specific discretization of the equations, but heuristically depends on the existence of a small parameter. The latter is typically derived from an anisotropy inherent in the problem. This could be due to many causes, but to appeal to the interests of the author's own research, we will focus on an anisotropy in the geometry of the domain and numerical discretization. However, it is easy to generalize the foregoing argument regardless of the actual source of anisotropy. Naively, the aspect ratio of the domain could be used to define such a parameter. However, the following example shows that it must also depend on the details of the discretization.

Suppose we want to solve the isotropic, 2D Poisson equation in a rectangular domain. We will choose a uniform discretization with  $N_x \times N_z$  cell-centers and we will define the aspect ratio to be  $\alpha = H/L$ . Upon switching to the dimensionless variables  $\tilde{x} = x/L$  and  $\tilde{z} = z/H$ , Poisson's equation transforms as follows

$$\begin{aligned} \rho &= \left( \frac{\partial^2}{\partial x^2} + \frac{\partial^2}{\partial z^2} \right) \phi \\ &= \frac{1}{H^2} \left( \alpha^2 L^2 \frac{\partial^2}{\partial x^2} + H^2 \frac{\partial^2}{\partial z^2} \right) \phi \\ &= \frac{1}{H^2} \left( \alpha^2 \frac{\partial^2}{\partial \tilde{x}^2} + \frac{\partial^2}{\partial \tilde{z}^2} \right) \phi \end{aligned}$$

We will rescale the field variable,  $\phi$ , so that it is dimensionless and of  $\mathcal{O}(1)$ , which is always possible. Now, apart from an overall scaling of  $H^{-2}$ , it is natural to identify the small parameter  $\varepsilon$  with the aspect ratio of the grid. However, a little reflection shows that a more “quantitative” definition of  $\varepsilon$  cannot ignore the discretization altogether. Indeed, once discretized, the term involving  $x$ -derivatives is at most  $\sim \alpha^2 N_x^2$  while the term involving  $z$ -derivatives is at least  $\sim 1$ . This means that if  $\alpha N_x \ll 1$ , then  $\frac{\partial^2 \phi}{\partial x^2}$  will be fundamentally smaller than  $\frac{\partial^2 \phi}{\partial z^2}$ , and so the “smallness” of  $\varepsilon$  depends on both the aspect ratio of the domain

and on the details of its discretization. It follows that, in the continuum limit,  $\varepsilon$  cannot be *a priori* ever guaranteed to be small.

Scotti and Mitran quantified these results in a more general manner. In their paper [10], they define the grid’s *leptic ratio*,  $\lambda = \min(\Delta x^m/H)$ , where  $\min \Delta x^m$  is the minimum grid spacing in the directions other than the vertical. Note that the leptic ratio is controlled by the overall aspect ratio of the domain and by the degree of “coarseness” of the discretization in the horizontal directions. It is shown that if  $\lambda > \mathcal{O}(1)$ , then the computational grid is “thin,” and the summarized equations of the previous section will indeed produce solutions whose sum converges to the solution of (1). This result extends to more exotic, N-dimensional geometries if we identify the symmetric tensor field,  $\sigma^{ij}$ , with  $\sqrt{g}g^{ij}$ .

At first, it would seem that this method is of very limited practical utility, being convergent only on rather coarse grids. Moreover, it is at odds with the very sensible idea that finer grids should lead to better results. However, in this article we pursue the idea that even when the leptic ratio of the grid is below critical, so that the expansion will not converge, the method can still be used to accelerate the convergence of conventional methods. Loosely speaking, the idea is that the r.h.s. can be partitioned between a component that can be represented on a grid with  $\lambda > 1$  and a remainder which needs a finer grid with  $\lambda < 1$ . Restricted to the former component, the expansion converges, while it diverges on the latter. On the contrary, traditional method such as BiCGStab tend to converge fast on the latter, and slow on the former. By judiciously blending both methods, we can achieve a uniformly high level of convergence. Also, note that since the expansion is formulated analytically, it can be implemented regardless of any particular choice of discretization of the domain. In the following examples, we will use a second-order scheme on a staggered grid, but the method is by no means restricted to this type of discretization.

### 3. Convergence estimates

#### 3.1. Restricted case

The heuristic arguments used earlier can be given an analytic justification in the case of a simple rectangular geometry. Once again, we limit to two dimensions, the extension to higher dimensional spaces being trivial. The elliptic equation we wish to solve is

$$(\partial_x^2 + \partial_z^2) \phi(x, z) = \rho(x, z) \quad (16)$$

with homogeneous Neumann boundary conditions. Without loss of generality, we can set  $\rho(x, z)$  equal to an arbitrary eigenfunction of the operator,  $\cos(kx) \cos(mz)$ . The exact, analytic solution of eq. (16) becomes simply

$$\phi(x, z) = -\frac{\cos(kx) \cos(mz)}{k^2 + m^2}.$$

Now, let's investigate how the leptic solver would have arrived at a solution.

First, we will write eq. (16) as

$$(\varepsilon \partial_x^2 + \partial_z^2) (\phi_0 + \varepsilon \phi_1 + \dots) = \cos(kx) \cos(mz), \quad (17)$$

where the  $\varepsilon$  is only used to identify small terms and will eventually be set to 1.

Equating various powers of  $\varepsilon$  gives us

$$\begin{aligned} \partial_z^2 \phi_0 &= \cos(kx) \cos(mz) \\ \partial_z^2 \phi_1 &= -\partial_x^2 \phi_0 \\ \partial_z^2 \phi_2 &= -\partial_x^2 \phi_1 \\ &\text{etc} \dots \end{aligned}$$

The solution to the  $\mathcal{O}(1)$  equation is

$$\phi_0(x, z) = \frac{\cos(kx) \cos(mz)}{-m^2}.$$

The constant of integration, that is  $\phi_0^h(x)$ , is identically zero since the BCs are homogeneous and there is no need for an excess function. The  $\mathcal{O}(\varepsilon)$  equation becomes

$$\partial_z^2 \phi_1 = -\frac{k^2}{m^2} \cos(kx) \cos(mz)$$

whose solution is

$$\phi_1(x, z) = -\frac{k^2}{m^2} \frac{\cos(kx) \cos(mz)}{-m^2}.$$

Continuing in this manner, we see that the solution at  $\mathcal{O}(\varepsilon^n)$  is

$$\phi_n(x, z) = \left(-\frac{k^2}{m^2}\right)^n \frac{\cos(kx) \cos(mz)}{-m^2}$$

which means that if we terminate the leptic solver at  $\mathcal{O}(\varepsilon^p)$ , the solution we arrive at is given by the sum

$$\phi(x, z) = \frac{\cos(kx) \cos(mz)}{-m^2} \sum_{n=0}^p \left(-\frac{k^2}{m^2}\right)^n \quad (18)$$

where we have set  $\varepsilon$  to 1. If  $k^2/m^2 \geq 1$ , then this geometric series will diverge as  $p \rightarrow \infty$  and the leptic solver will ultimately fail. On the other hand, if  $k^2/m^2 < 1$ , then the series will be finite for all values of  $p$  and we can put the solution in a closed form,

$$\phi(x, z) = \frac{\cos(kx) \cos(mz)}{-(k^2 + m^2)} \left\{ 1 - \left(-\frac{k^2}{m^2}\right)^{p+1} \right\}.$$

In the limit  $p \rightarrow \infty$ , the term in braces tends to 1 and we recover the exact, analytic solution of the elliptic equation.

Since the wavenumbers  $k$  and  $m$  are both positive, we can simply say that convergence of the leptic method requires  $\max(k/m) < 1$ . Analytically, this quantity depends on the harmonic content of the source,  $\rho(x, z)$ , and is, in principle, unbounded. Numerically, once a discretization has been chosen,  $k$  and  $m$  are limited to a finite number of values. If we let the source term be a general linear combination of eigenfunctions and if our rectangular domain has dimensions  $L$  by  $H$  divided uniformly into elements of size  $\Delta x$  by  $\Delta z$ , and it is discretized with a spectral method, then  $\max(k) = \pi/\Delta x$  and  $\min(m) = \pi/H$ . This produces our convergence condition,  $H/\Delta x < 1$ , which is the origin of the leptic ratio,  $\lambda = \min(\Delta x^m/H)$ , and its square inverse,  $\varepsilon = \max(H/\Delta x^m)^2$ , used throughout this paper.

Notice that this convergence condition is a restriction on how we must discretize a given domain, it is not directly a restriction on the source term of the

elliptic equation at hand. This means that the leptic method should converge similarly for all equations that use a particular uniform, rectangular grid. If the grid is not rectangular or uniform, then the relevant convergence condition is  $H_i/\Delta x_i < 1$  at all grid positions,  $i$ . Here,  $H_i$  is the vertical height of the domain at  $x_i$  and  $\Delta x_i$  is the minimum horizontal grid spacing at  $x_i$ .

### 3.2. General case

Now, we will extend this argument to the more general case involving the positive-definite, symmetric tensor field,  $\sigma^{ij}(x, z)$ . We wish to perform a convergence analysis on

$$\{\partial_z \sigma^{zz} \partial_z + \varepsilon (\partial_x \sigma^{xx} \partial_x + \partial_x \sigma^{xz} \partial_z + \partial_z \sigma^{zx} \partial_x)\} \phi(x, z) = \rho(x, z). \quad (19)$$

Without the exact form of each  $\sigma^{ij}(x, z)$ , we cannot trivially diagonalize the operator in  $(k, m)$ -space. We can, however, diagonalize the operator in  $(x, z)$ -space by performing a small rotation by an angle  $\frac{1}{2} \tan^{-1} \left( \frac{2\varepsilon \sigma^{xz}}{\sigma^{zz} - \varepsilon \sigma^{xx}} \right)$ . This casts the equation into the simpler form

$$\{\partial_z [\sigma^{zz} + \mathcal{O}(\varepsilon^2)] \partial_z + \partial_x [\varepsilon \sigma^{xx} + \mathcal{O}(\varepsilon^2)] \partial_x\} \phi(x, z) = \rho(x, z),$$

where the  $x$  and  $z$  now represent the new coordinates. We might as well just let  $\sigma^{zz} + \mathcal{O}(\varepsilon^2) \rightarrow \sigma^{zz}$  and  $\varepsilon \sigma^{xx} + \mathcal{O}(\varepsilon^2) \rightarrow \varepsilon \sigma^{xx}$  so that

$$\{\partial_z \sigma^{zz} \partial_z + \varepsilon \partial_x \sigma^{xx} \partial_x\} \phi(x, z) = \rho(x, z). \quad (20)$$

Even though each term of eq. (20) is functionally different than the corresponding terms of eq. (17), their magnitudes are equal. This means that a convergence analysis of eq. (20) must lead to a restriction of the form  $\lambda > \mathcal{O}(1)$ . Rotating back to eq. (19) cannot possibly change this restriction due to the vanishing size of the rotation angle. This shows that even in the general case of eq. (1), the leptic solver will converge as long as the discretization is chosen to satisfy  $\lambda > \mathcal{O}(1)$ .

### 3.3. The leptic solver as a preconditioner

Let us return to the simple case of solving  $\nabla^2 \phi = \cos(kx) \cos(mz)$  on a rectangular domain. After applying  $n_l$  iterations of the leptic solver, the residual,  $r$ , is found via eq. (18) with  $p = n_l - 1$ .

$$\begin{aligned}
r &= \cos(kx) \cos(mz) - \nabla^2 \left\{ \frac{\cos(kx) \cos(mz)}{-m^2} \sum_{n=0}^{n_l-1} \left( -\frac{k^2}{m^2} \right)^n \right\} \\
&= \cos(kx) \cos(mz) - \frac{k^2 + m^2}{m^2} \cos(kx) \cos(mz) \sum_{n=0}^{n_l-1} \left( -\frac{k^2}{m^2} \right)^n \\
&= \left\{ 1 + \sum_{n=1}^{n_l} \left( -\frac{k^2}{m^2} \right)^n - \sum_{n=0}^{n_l-1} \left( -\frac{k^2}{m^2} \right)^n \right\} \cos(kx) \cos(mz) \\
&= \left( -\frac{k^2}{m^2} \right)^{n_l} \cos(kx) \cos(mz)
\end{aligned}$$

The last line comes from collapsing the telescoping set of sums. This gives us an amplification factor for each eigenmode of the residual. That is, if we are given a generic residual and perform an eigenvector expansion,

$$r(x, z) = \sum_k \sum_m r(k, m) \cos(kx) \cos(mz),$$

then the magnitudes of the individual components,  $r(k, m)$ , will be amplified or attenuated by  $k^2/m^2$  each time we iterate. If the grid is constructed such that  $\lambda > \mathcal{O}(1)$ , then  $r(k, m)$  will always be attenuated since  $\max(k^2/m^2) < 1$ . If, however, the grid's leptic ratio is  $\sim \mathcal{O}(1)$ , then only those eigenmodes with  $k^2/m^2 < 1$  will diminish and those with  $k^2/m^2 > 1$  will be amplified. In  $(x, z)$ -space, this effect appears as a diverging solution, but in  $(k, m)$ -space, we can see that the solution is split into converging and diverging parts – we are conditioning the solution. For this reason, even though preconditioning is normally understood as the action of substituting the original operator with a modified one with better spectral properties [15], we will use preconditioning to mean the action of replacing an initial guess with one that has better spectral support.

As an example, consider a  $64 \times 64 \times 16$  grid with  $\Delta x = (1, 1, 0.1)$ . This fixes

$\varepsilon$  at 2.56, which is large enough to cause problems for the leptic solver.<sup>3</sup> In order to learn how the solvers are treating the modes on this grid, let's apply them to

$$\nabla^2 \phi = \sum_{i=1}^{32} \sum_{j=1}^{32} \sum_{k=1}^8 \cos\left(\frac{2\pi i x}{L}\right) \cos\left(\frac{2\pi j y}{L}\right) \cos\left(\frac{2\pi k z}{H}\right)$$

with homogeneous boundary conditions. This is a residual equation whose r.h.s. harbors every periodic mode supported by the grid in equal amounts (except for the zero modes, which must be removed to be consistent with the boundary conditions). We only consider periodic modes to facilitate spectral analysis via FFT. In one test, we solved this equation with a BiCGStab solver and in another separate test, we used the leptic method. BiCGStab stalled in 26 iterations and the leptic solver began to diverge after 24 iterations. Once progress came to a halt, we performed an FFT to locate which modes were converging slowest. To simplify the visualization, we found the  $(k_x, k_y)$  slice that contained the most slowly converging modes (which, consistent with the previous analysis, is the smallest value  $k_z = 2\pi/H$ ). The results are in figures 2 and 3.<sup>4</sup>

The color in these plots represent the base-10 logarithm of the Fourier coefficients of each mode. It is apparent that each method has its own distinct problem region shown in red. The BiCGStab solver has the most trouble dealing with low frequency modes while the leptic solver has trouble with high frequency modes. Since the leptic solver produced a residual whose largest modes can easily be handled by BiCGStab, we apply the BiCGStab using as initial guess the output of the leptic solver after 18 iterations. Now BiCGStab is able to converge quickly (figure 4).

We should mention that this is just an illustration. In this example, the BiCGStab method on such a small grid would have converged on its own in a reasonable number of iterations. On a larger grid, BiCGStab alone often

---

<sup>3</sup>For the remainder of this paper, we will be dealing with a geometric anisotropy quantified by  $\lambda$ . The perturbation parameter is then  $\varepsilon = (H/\Delta x)^2$ .

<sup>4</sup>VisIt has been developed and is being distributed by the Lawrence Livermore National Laboratory. Website: <https://wci.llnl.gov/codes/visit>.

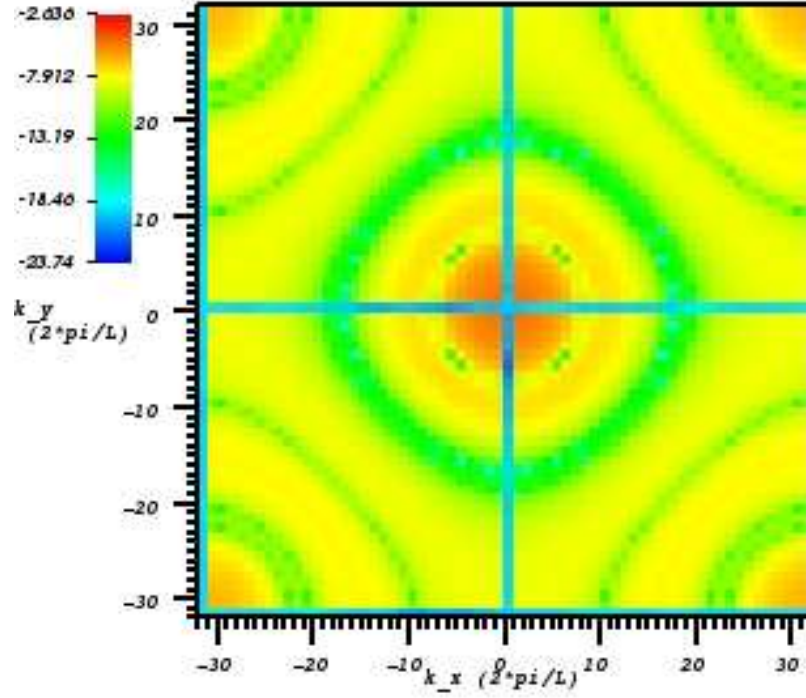


Figure 2: A 2-dimensional slice of the residual error after 26 iterations of BiCGStab. Colors are on a logarithmic scale. Notice the large error near the center of the plot, indicating BiCGStab's difficulty eliminating low frequency errors. The blue lines are the zero-frequency modes that must be fixed to agree with the boundary conditions.

converges too slowly to be a viable solution method and sometimes stalls due to the condition number of the operator. Further complications arise when we use mapped coordinates because this tends to drive the condition number of the operator even higher. In these situations, using the leptic method to generate a suitable initial guess becomes quite useful. We will illustrate this effect in further detail in section 4.



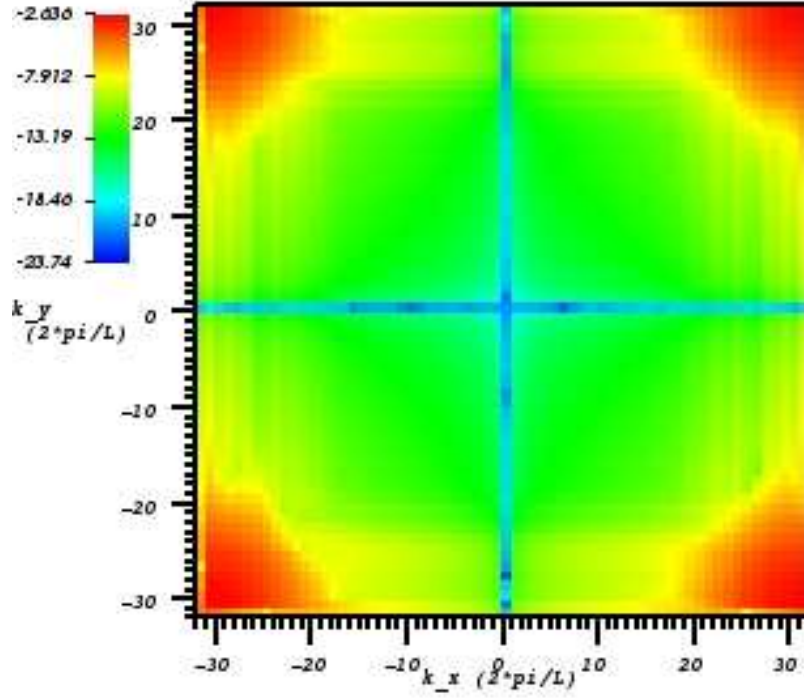


Figure 3: The residual error after 24 iterations of the leptic solver. This solver eliminates low frequency errors much more effectively than high frequency errors, indicating the leptic solver's potential to serve as a preconditioner for BiCGStab.

#### 4. Demonstrations

In this section, we will create a sample problem on various numerical domains in order to compare the effectiveness of traditional solvers with methods that utilize the leptic solver. Our traditional solver of choice will be the BiCGStab method preconditioned with the incomplete Cholesky factorization (IC) of the elliptic operator [12]. For simplicity, we will use a rectangular domain and the

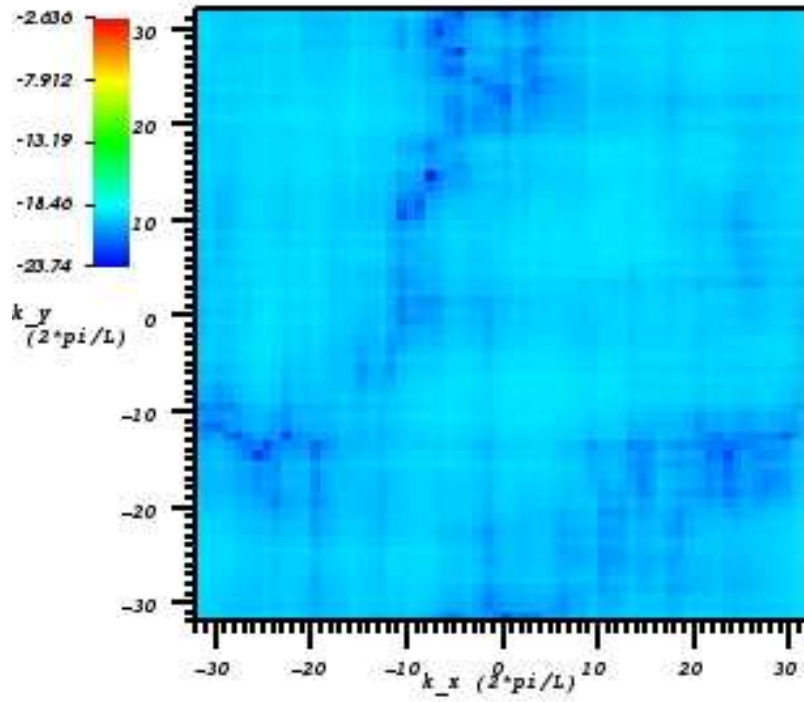


Figure 4: The residual error of the BiCGStab method when given an initial guess generated by the leptic solver.

r.h.s. will be generated by taking the divergence of a vector field

$$\begin{aligned}
 u^{*1} &= \left(\frac{z}{L_z}\right)^2 \sin\left(\frac{\pi y}{L_y}\right) + \frac{x}{\sqrt{2}L_z} \\
 u^{*2} &= \left(\frac{z}{L_z}\right)^2 \sin\left(\frac{\pi x}{L_x}\right) \\
 u^{*3} &= -\left(\frac{z}{L_z}\right)^2 \cos\left(\frac{\pi z}{4L_z}\right) \\
 \rho &= \partial_i u^{*i}.
 \end{aligned}$$

This vector field also generates the boundary conditions. To compare the solvers, we will plot the relative residual as a function of the iteration number. For what follows, the vertical and horizontal solves of the leptic solver will each be counted each as an iteration.

#### 4.1. High leptic ratio - Cartesian coordinates

First, we set  $N = (64, 64, 16)$  and  $\Delta x = (0.1, 0.1, 0.001)$ . This fixes  $\varepsilon$  at 0.0256, which lies well within the region where the leptic solver outperforms traditional methods. Figure 5 shows the results. The leptic solver is clearly the more efficient method. In only 6 iterations, it is able to achieve a relative residual of  $10^{-10}$ . We would have needed 170 iterations of the BiCGStab/IC solver to obtain a residual error of that magnitude.

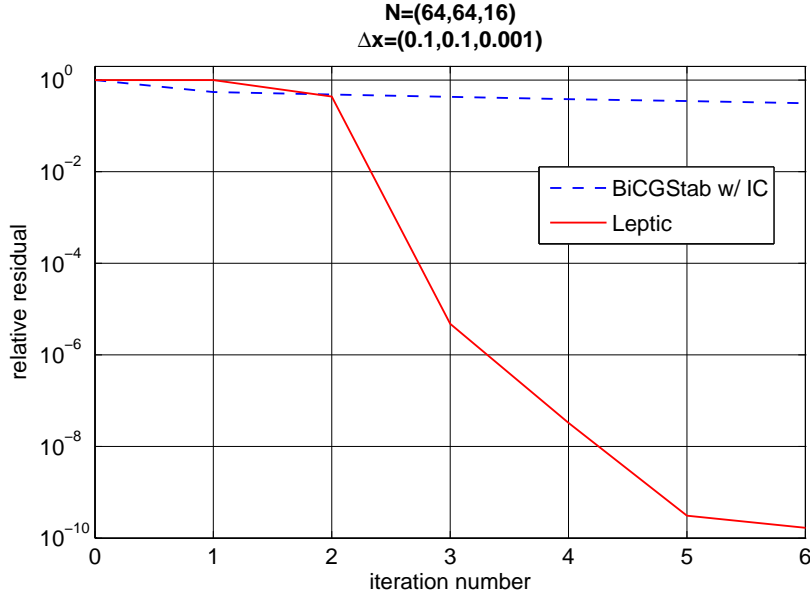


Figure 5: With  $\varepsilon \approx 1/40$ , the leptic solver is clearly more efficient than BiCGStab. Since we are using Cartesian coordinates, the leptic solver only needed to perform one horizontal solve.

#### 4.2. Borderline cases - Cartesian coordinates

When  $\varepsilon = \mathcal{O}(1)$ , the leptic solver may or may not be the most efficient solver. We will denote these situations as *borderline cases*. In the first borderline case, we will bring  $\varepsilon$  to 1 by setting  $N = (64, 64, 10)$  and  $\Delta x = (0.1, 0.1, 0.01)$ . Figure 6 shows that the leptic solver requires approximately 5 times as many iterations as it did in the  $\varepsilon = 0.0256$  example to achieve an  $\mathcal{O}(10^{-10})$  residual

error. The BiCGStab/IC method, however, converges a bit more quickly than it did in the previous example. It required only 90 iterations to catch up to the leptic method. This is empirical evidence of our theoretical assertion – by raising  $\varepsilon$  (decreasing the lepticity), the leptic solver becomes less effective and the traditional method becomes more effective. In this specific borderline case, the leptic solver outperforms the BiCGStab method.

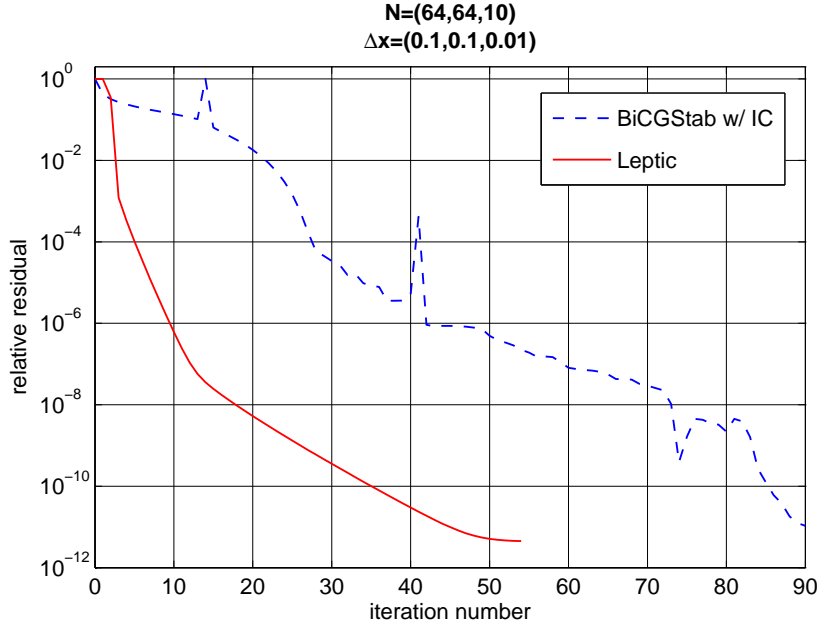


Figure 6: The convergence patterns of the leptic and BiCGStab solvers when  $\varepsilon = 1$  and condition number  $\approx 10^{5.6}$ . The spikes in the BiCGStab residual are due to restarts.

By varying  $N_x$  and  $N_y$ , we can generate an entire class of grids with the same  $\varepsilon$ . For example, if we bring  $N$  up to  $(256, 256, 10)$ , the BiCGStab method should not converge as rapidly as before. On the other hand,  $\varepsilon$  is still 1, which means the leptic solver should perform almost as well as it did on the  $64 \times 64 \times 10$  grid. This is because most of the leptic solver’s convergence relies on the vertical solver. This is true in general when the horizontal solver is able to be switched off (see section 2.3) – as the horizontal domain grows, the leptic solver outperforms traditional relaxation methods. This effect is shown in figure 7. By comparing

figures 6 and 7, we see that unlike the leptic method, the BiCGStab/IC method is in fact slowed down by the larger horizontal grid.

The true value of the leptic solver is illustrated by when we use it to generate a suitable initial guess for the BiCGStab/IC solver (see section 3.3). This initial guess has an error that is dominated by high wavenumbers. The BiCGStab solver then rapidly removes those errors as shown by the dash-dot curve in figure 7.

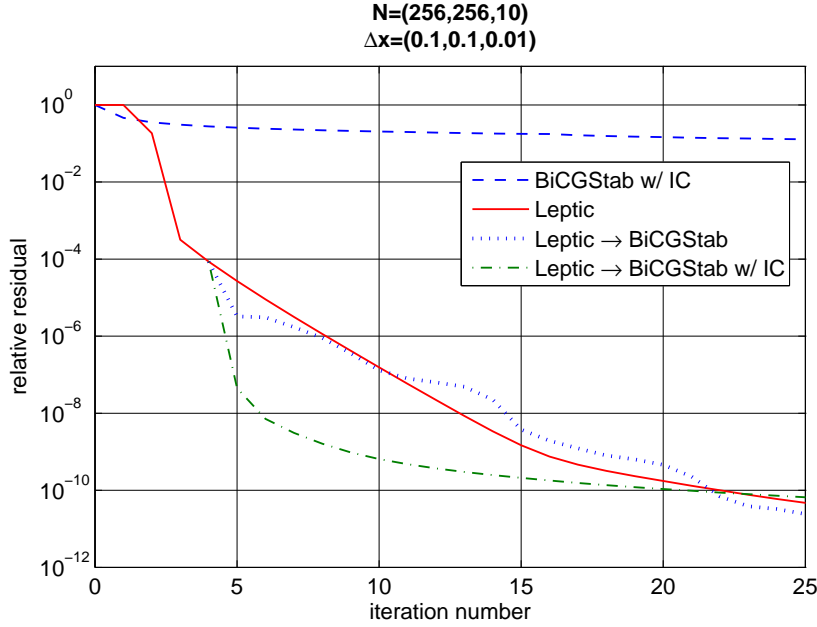


Figure 7: The performance of various solution methods with  $\varepsilon = 1$  and condition number  $\approx 10^{6.8}$ . After a few iterations of the leptic solver, BiCGStab can achieve a fast convergence rate. Using a preconditioner such as an incomplete Cholesky decomposition can drive this rate even higher.

As our final isotropic, borderline case, we will set  $N = (50, 50, 50)$  and  $\Delta x = (0.1, 0.1, 0.004)$ . This is appropriate for a cubic, vertically stratified domain and brings  $\varepsilon$  up to 4. The BiCGStab/IC solver does not provide immediate convergence and the leptic method would have started to diverge after its third iteration, but when we combine the two methods as we did in the last example,

we see a much more rapid convergence than either method could individually achieve (figure 8).

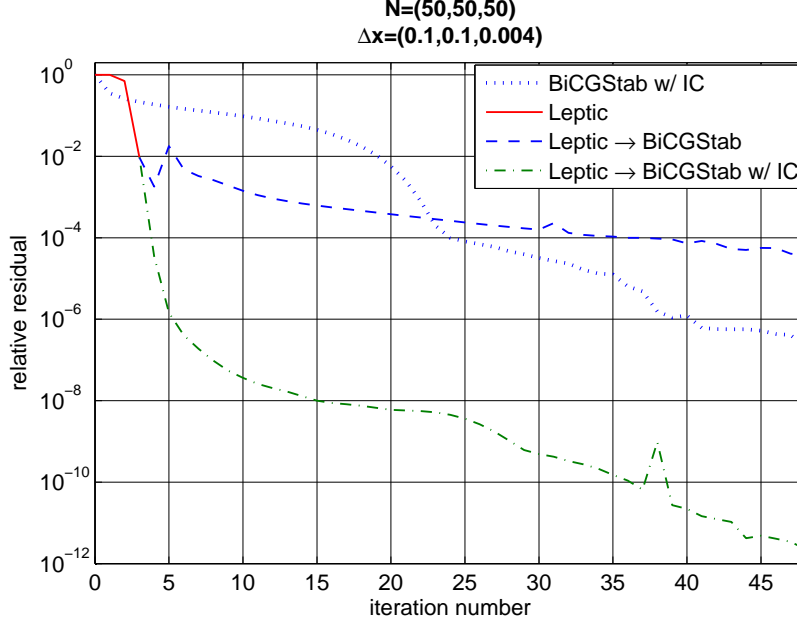


Figure 8: Performance of the solvers with  $\varepsilon = 4$  and condition number  $\approx 10^{6.2}$ . The leptic solver began diverging after it's third iteration, so control was passed to the Krylov solver. Again, the leptic solver proves most valuable as a preconditioner for the BiCGStab/IC solver when  $\varepsilon = \mathcal{O}(1)$ .

#### 4.3. High leptic ratio - Mapped coordinates

When the metric is diagonal, several of the terms in our expansion (sec. 2.2) vanish. This means we can remove much of the code to produce a more efficient algorithm. This reduced code is what generated the results of the previous sections. However, in these simple geometries the value of the leptic expansion is somewhat limited because it is normally possible to employ fast direct solvers. Not so in the case we consider now, where we apply the full algorithm by considering a non-diagonal metric. The metric we will use is routinely employed in meteorological and oceanic simulations of flows over non uniform terrain. It

maps the physical domain characterized by a variable topography  $z = h(x, y)$  to a rectangular computational domain. Although any relief may be specified, it is sufficient for our illustrative purposes to simply let the depth go from  $d/2$  to  $d$  linearly as  $x$  goes from 0 to  $L$ , where  $d < 0$  (Figure 9).

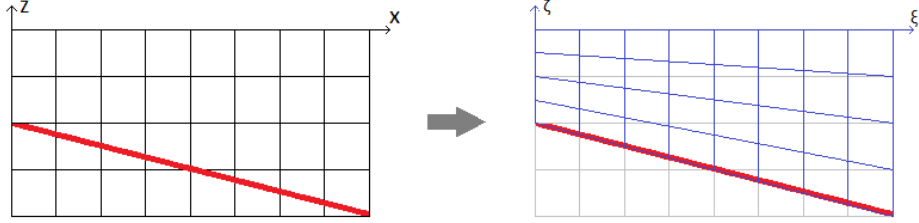


Figure 9: A cross section of the coordinate mapping. The thick line denotes the lower vertical boundary.

We define  $h(\xi) = \frac{d}{2} + \frac{d}{2L}\xi$ , where  $(x, y, z) \rightarrow (\xi, \eta, \frac{h(\xi)}{d}\zeta)$ . This means that the symmetric tensor,  $\sigma^{ij} = \sqrt{g}g^{ij}$ , is given by

$$\sqrt{g}g^{ij} = \begin{pmatrix} \frac{\xi+L}{2L} & 0 & -\frac{\zeta}{2L} \\ 0 & \frac{\xi+L}{2L} & 0 \\ -\frac{\zeta}{2L} & 0 & \frac{4L^2+\zeta^2}{2L(\xi+L)} \end{pmatrix}^{ij}.$$

For the next two examples, we will be seeking a simple

$$\phi_{\text{sol}}(\xi, \eta, \zeta) = \cos\left(\frac{2\pi\xi}{L}\right) \cos\left(\frac{2\pi\eta}{L}\right) \cos\left(\frac{2\pi\zeta}{d}\right)$$

solution by setting  $u^{*i} = \sqrt{g}g^{ij}\partial_j\phi_{\text{sol}}$  and  $\rho = \partial_i u^{*i}$ .

Setting  $N = (256, 256, 64)$  and  $\Delta x = (0.25, 0.25, 0.0025)$  gives us  $\varepsilon = 0.4096$ . After approximately 200 iterations, the BiCGStab method begins to stall with a relative residual of  $\mathcal{O}(10^{-8})$ . On the other hand, the leptic solver was able to reach a relative residual of  $3.637 \times 10^{-9}$  in only 10.2% of the time before terminating at  $\mathcal{O}(\varepsilon^4)$ . The reason the leptic method stopped iterating was due to inconsistent data given to the vertical solver. In section 2, we showed that at each iteration, a 2D poisson problem, namely eq. (11), must be handed to a traditional solver and if that solver fails, the next vertical stage may have a source

term that is not compatible with its boundary conditions. Remarkably, the horizontal stages failed (abandoned due to stalling) at every order of calculation and the leptic solver was still able to out-perform the BiCGStab method. Had our decision-making algorithm been altered to abandon the horizontal solver after failing the first time, which is reasonable for some problems, we would have converged much faster. It should be pointed out that until  $\mathcal{O}(\varepsilon^4)$ , the leptic solver did not diverge, therefore we never needed to transfer control to a full 3D BiCGStab solver – which would have been slow.

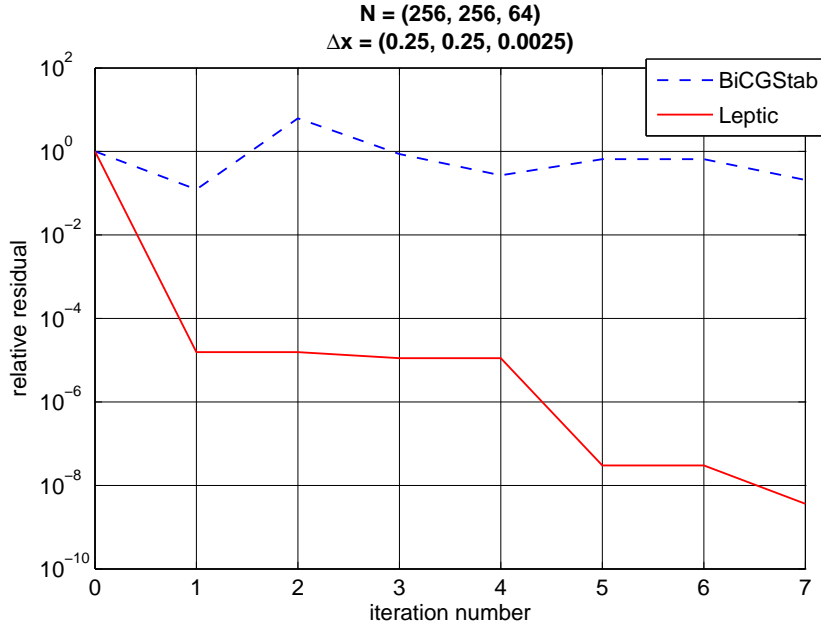


Figure 10: Performance of the leptic and Krylov solvers with an anisotropic  $\sigma^{ij}$  and  $\varepsilon \approx 0.4$ . Since our solver is using Chombo’s matrix-free methods (known as *shell matrices* in some popular computing libraries such as PETSc [16]), the Cholesky decomposition of the elliptic operator can not be performed.

#### 4.4. Borderline case - Mapped coordinates

For this scenario, we set  $N = (64, 64, 10)$  and  $\Delta x = (0.5, 0.5, 0.1)$  giving us  $\varepsilon = 4$ . To solve our sample problem on this grid, we let the leptic and BiCGStab



solvers work together, iteratively. As soon as one solver begins to stall or diverge, control is passed to the other solver. The effectiveness of this algorithm is explained in section 3.3 – the leptic solver first reduces low frequency errors until high frequency errors begin to dominate the residual, then the BiCGStab solver reduces high frequency errors until low frequency errors dominate the error. This continues until the residual error has been reduced over the entire spectrum supported by the grid. Figure 11 illustrates the effectiveness of this algorithm rather convincingly.

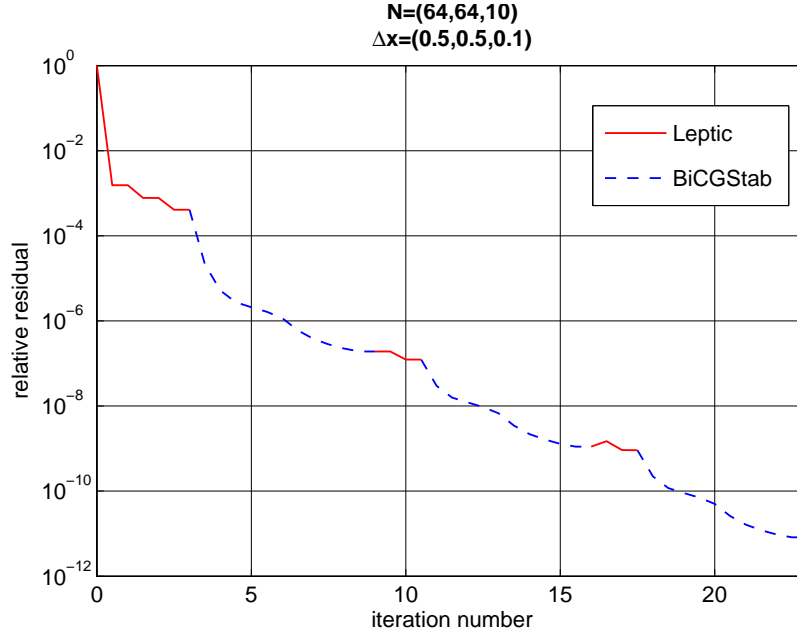


Figure 11: The convergence pattern of a hybrid leptic/Krylov method when  $\varepsilon = 4$  on an anisotropic domain. In this case, neither method would have individually provided rapid convergence, but when the methods are combined, we see a very rapid convergence and the introduction of another preconditioner (eg. IC) is not necessary.

## 5. Discussion

The leptic method was originally devised as a method to add a physically appropriate amount of dispersion when numerically modeling the propagation

of nonlinear waves in a dispersive medium. In this paper, we generalized the method so it could be used to actually speed up the numerical solution of Poisson problems characterised by a high level of anisotropy. The key idea is that instead of (or in addition to) preconditioning the operator to achieve overall better spectral properties, we precondition the initial guess (or the restarts) to achieve better spectral support of the residual by coupling the leptic expansion to Krylov methods. However, since the former converges on its own if the lepticity of the grid is sufficiently large, it is easy to see that it could be used within multigrid methods as well. Namely, when the coarsening reaches a point that the lepticity of the grid is below critical, the leptic expansion can be used in lieu of the relaxing stage to generate an exact solution at the coarse level. This would likely cut down the layers of coarsening.

In its full generality, this method can be used to solve anisotropic Poisson equations in arbitrary,  $D$ -dimensional coordinate systems. In many cases, however, numerical analysis is performed using simple, rectangular coordinates without an anisotropic tensor,  $\sigma^{ij}$ . This simplification reduces much of the computation. For these common purposes, we included a summary of the Cartesian version of the expansion. Both the general and Cartesian expansions are summarized in section 2.2.

When implementing the leptic method for numerical work, the computational domain should be split in all but the vertical (stiff) dimension. The vertical ordinary differential equations require a set of integrations – one for each point in the horizontal plane. With this domain decomposition, these integrations are independent of one another and the solutions to the vertical problems can be found via embarrassingly parallel methods. On the other hand, the solutions to the horizontal equations cannot be parallelized as trivially, making their solutions more costly to arrive at. In light of this, section 2.3 was provided to discuss when it is appropriate to eliminate these expensive stages.

The computational cost of a single iteration is of the same order as a preconditioned step of a Krylov method. The savings are obtained in the faster rate of convergence, shown in the examples above over a wide range of anisotropic

conditions, as well as the relative ease with which the leptic expansion can be parallelized. The best rate of convergence is achieved by using the leptic expansion at the beginning and every time the convergence rate of the Krylov method slows down. We did not attempt to predict a priori after how many steps the switch is necessary. If the Poisson problem, as it often happens, is part of a larger problem that is solved many times, a mockup problem should be solved at the beginning to determine empirically the best switch pattern.

Adapting the expansion to accept Dirichlet boundary conditions would require a new derivation similar to that of section 2, but the job would be much simpler since Dirichlet elliptic operators have a trivial null space, thereby eliminating the need to consider compatibility conditions among the second-order operators and their boundary conditions.

**Acknowledgment:** This work was supported by grants from ONR and NSF.

## References

- [1] D. L. Brown, R. Cortez, M. L. Minion, Accurate projection methods for the incompressible navier-stokes equations, *Journal of Computational Physics* 168 (2001) 464–499.
- [2] J. H. Ferziger, M. Peric, *Computational Methods for Fluid Dynamics*, Springer-Verlag, 3rd edition, 2001.
- [3] J. W. Demmel, *Applied Numerical Linear Algebra*, SIAM, 1997.
- [4] O. Fringer, M. Gerritsen, R. Street, An unstructured-grid, finite-volume, nonhydrostatic, parallel coastal ocean simulator, *Ocean Modelling* 14 (2006) 139–173.
- [5] J. Binney, S. Tremaine, *Galactic Dynamics*, Princeton University Press, 2nd edition, 1988.
- [6] S. M. Hassanizadeh, On the transient non-fickian dispersion theory, *Transport in Porous Media* 23 (1996) 107–124.
- [7] S. A. Cummer, B.-I. Popa, D. Schurig, D. R. Smith, J. Pendry, M. Rahm, A. Starr, Scattering theory derivation of a 3d acoustic cloaking shell, *Phys. Rev. Lett.* 100 (2008) 024301.
- [8] D. R. Smith, D. Schurig, J. J. Mock, Characterization of a planar artificial magnetic metamaterial surface, *Phys. Rev. E* 74 (2006) 036604.
- [9] V. Armenio, F. Roman, Large eddy simulation of environmental shallow water coastal flows, *ERCOFTAC Bulletin* 78 (2009) 46–53.
- [10] A. Scotti, S. Mitran, An approximated method for the solution of elliptic problems in thin domains: Application to nonlinear internal waves, *Ocean Modelling* 25 (2008) 144–153.
- [11] A. M. Bruaset, A. Tveito, A numerical study of optimized sparse preconditioners, *BIT Numerical Mathematics* 34 (1994) 177–204. 10.1007/BF01955867.

- [12] K. Teranishi, P. Raghavan, A hybrid parallel preconditioner using incomplete cholesky factorization and sparse approximate inversion, in: T. J. Barth, M. Griebel, D. E. Keyes, R. M. Nieminen, D. Roose, T. Schlick, O. B. Widlund, D. E. Keyes (Eds.), *Domain Decomposition Methods in Science and Engineering XVI*, volume 55 of *Lecture Notes in Computational Science and Engineering*, Springer Berlin Heidelberg, 2007, pp. 755–762.
- [13] J. Boussinesq, Théorie des ondes et des remous qui se propagent le long d’un canal rectangulaire horizontal, en communiquant au liquide contenu dans ce canal des vitesses sensiblement pareilles de la surface au fond, *Journal de Mathématique Pures et Appliquées* (1872) 55–108.
- [14] T. F. Chan, H. C. Elman, Fourier analysis of iterative methods for elliptic problems, *SIAM Review* 31 (1989) 20–49.
- [15] H. A. van der Vorst, *Iterative Krylov Methods for Large Linear Systems*, Cambridge Monographs on Applied and Computational Mathematics, Cambridge University Press, 2003.
- [16] S. Balay, J. Brown, K. Buschelman, W. D. Gropp, D. Kaushik, M. G. Knepley, L. C. McInnes, B. F. Smith, H. Zhang, PETSc Web page, 2011. [Http://www.mcs.anl.gov/petsc](http://www.mcs.anl.gov/petsc).